Available online at www.sciencedirect.com
SCIENCE DIRECT®
Journal of Molecular Catalysis A: Chemical 228 (2005) 325–331
JOURNAL OF MOLECULAR CATALYSIS A: CHEMICAL
www.elsevier.com/locate/molcata

Perovskites as catalysts precursors: synthesis and characterization

M.R. Goldwasser[a,*], M.E. Rivas[a], E. Pietri[a], M.J. Pérez-Zurita[a], M.L. Cubeiro[a], A. Grivobal-Constant[b], G. Leclercq[b]

[a] *Centro de Catálisis, Petróleo y Petroquímica, Escuela de Química, Facultad de Ciencias, Universidad Central de Venezuela, Apartado 47102, Los Chaguaramos, Caracas, Venezuela*
[b] *Université des Sciences ET Technologies de Lille, Laboratoire de Catalyse Hétérogène et Homogène, 59655 Villeneuve D'Ascq Cedex, France*

Available online 5 November 2004

Abstract

Perovskites type oxides $La_{1-x}Ca_xRu_{1-x}Ni_xO_3$ were synthesized by the citrate sol–gel method. Characterization was carried out underlying the modification of metal catalysts by promoters by total or partial substitution of A- and B-site cations. The influence of Ru partial substitution by Ni in the $LaRuO_3$ structure and of La by Ca on $LaRu_{0.8}Ni_{0.2}O_3$ was also investigated in the dry and combine reforming of methane. All perovskites series, showed a well-defined perovskite structure with surface areas between 2 and 17 m^2/g. After reduction Ru(Ni) crystallites size in the order of 10–15 nm were produced. An oxygen deficiency was shown by most perovskites. Substitution of La by Ca of smaller ionic radium decreases the stability of the perovskites and lowers their reduction temperature. Among the calcium series, $La_{0.8}Ca_{0.2}Ru_{0.8}Ni_{0.2}O_3$, proved to be the most active precursor catalyst with the highest selectivity to syngas. Correlation between the effect of partial or total substitution of La by Ca as A-site cation of the precursor perovskite, the catalytic activity and stability of in situ formed Ru(Ni) particles was established.

Keywords: CO_2 and combine reforming of methane; Syngas production; LaRuNi perovskites; Calcium promotion

1. Introduction

1.1. Perovskites

Complex mixed metal oxides with the perovskite structure and composition have long attracted the interest of chemists, as they exhibit interesting solid-state properties, making the structure very appropriate as model catalysts. The use of precursors such as perovskite-like oxides ABO_3, in which A-site cation is a rare earth and/or alkaline earth and B-site cation, is a transition metal has increased recently for methane reforming [1–5]. The ideal ABO_3 perovskite structure is cubic in which the larger A-site cation is surrounded by 12 oxygen and the smaller B-site cation by 6. One interesting feature of these complex mixed-oxides is that their catalytic activity can be highly improved by partial substitution on A- and/or B-sites, with only small changes in the average structure [1,6–9].

Perovskites not only fulfill the stability requirements for the reforming reactions, but also by further reduction of B-site cations which remain distributed in the structure, they form well dispersed and stable metal particle catalysts [1,2,8]. The use of perovskite allows stabilizing small particles of the metal in position B [Ru, Ni] over a stable support (Ca-, La-oxides) to prevent carbon formation in the reforming of methane. The reduced solids of nominal composition (Ru, Ni)/La_2O_3 and/or CaO, are used as catalysts to establish correlations between the effect of partial or total substitution of A- and B-site cations of the precursor perovskite and the catalytic activity and stability of in situ formed metallic particles.

1.2. Methane conversion to syngas

Even though steam reforming of methane is widely industrialized to produce syngas (a mixture of H_2 and CO), lower ratios are needed for oxo- and Fischer–Tropsch synthesis. Carbon dioxide reforming of methane offers advantages such

* Corresponding author. Fax: +58 212 239 21 62.
E-mail address: mgoldwas@reacciun.ve (M.R. Goldwasser).

1381-1169/$ – see front matter © 2004 Elsevier B.V. All rights reserved.
doi:10.1016/j.molcata.2004.09.030

as the production of syngas with a lower H_2/CO ratio and it obviates a water vaporization step to produce steam, an energy consumer process, and eliminate CH_4 and CO_2 two major greenhouse gases. Due to the high temperatures involved and the presence of steam, sinterization of the active metal species and coke formation lead to catalysts deactivation and in some cases to plugging of the reactor [10]. Methane conversion to syngas and H_2 based in steam reforming occurs by the two following reactions [11]:

$$CH_4 + H_2O \leftrightarrow CO + 3H_2 \quad (\Delta H_{298\,K} = 206\,kJ/mol) \quad (1)$$

$$CO + H_2O \leftrightarrow CO_2 + H_2 \quad (\Delta H_{298\,K} = -41\,kJ/mol) \quad (2)$$

These reactions produce syngas with a H_2/CO $\geq$3 ratio. However, carbon dioxide reforming of methane, yielding synthesis gas with low hydrogen to carbon monoxide ratio, has received renewed interests to transform CO_2 and CH_4 to more valuable products. Further transformations to produce methanol, higher alcohols and Fischer–Tropsch to diesel and light alkenes require H_2/CO $\leq$2 ratios, which can be accomplished by CO_2 dry reforming and by partial oxidation:

$$CH_4 + CO_2 \leftrightarrow 2CO + 2H_2 \quad (\Delta H_{298\,K} = 247\,kJ/mol) \quad (3)$$

$$CH_4 + \tfrac{1}{2}O_2 \leftrightarrow CO + 2H_2 \quad (\Delta H_{298\,K} = -36\,kJ/mol) \quad (4)$$

In these reactions, product distribution is thermodynamically controlled: H_2 is favored at high temperature (700–800 °C). However, to operate at high temperature introduces several potential problems:

- catalyst sintering enhanced by the presence of water vapor;
- catalyst stability;
- coke formation by the following two reactions:

$$CH_4 \leftrightarrow C + 2H_2 \quad (\Delta H_{298\,K} = +75\,kJ/mol) \quad (5)$$

$$2CO \leftrightarrow C + CO_2 \quad (\Delta H_{298\,K} = -173\,kJ/mol) \quad (6)$$

Coke formation via reaction (5) is favored at high temperature while reaction (6) is favored at low temperature [12]. Experimental operational conditions must then be carefully chosen to minimize coke formation.

In the present work, Perovskite-type based catalyst were developed to transform two cheap contaminating chemicals into more valuable feed stock and petrochemical such as syngas. Characterization was carried out to obtain a better appreciation of the principles underlying the modification of metal catalysts by promoters by total or partial substitution of A- and B-site cations. For comparison, some previous published results in the dry reforming of methane are included [1,2]. New results in the characterization and combine reforming of methane are also presented.

2. Experimental

The experimental part comprises the synthesis of perovskite-type oxides, the preparation of the catalysts, their characterization by different physico-chemical techniques and their performance in the dry and combines methane-reforming reactions.

2.1. Synthesis of perovskite-type oxides

Perovskites were synthesized by the citrate sol–gel method to ensure a good homogeneity of the mixed oxides. Adequate amounts of solutions of A- and B-site cations precursors were added to a solution of citric acid (99.5%, Riedel-de Haën) with an excess of ethylene glycol (99.5%, Riedel-de Haën) as the organic polydentate ligant as previously reported [1,2].

Adequate amounts of the precursor of the cation at B position were dissolved under vigorous stirring in a solution of citric acid (99.5%, Riedel-de Haën) with an excess of ethylene glycol (99.5%, Riedel-de Haën) as the organic polydentate ligant. The citric acid/B cation molar ratio was 4, while it was 1.38 for ethylene glycol/citric acid. The mixture was kept at 57 °C with mild continuous stirring until a clear solution was obtained. At this point, a stoichiometric quantity of the precursor of cation A, $La(NO_3)_3{\cdot}5H_2O$ or $Ca(NO_3)_2{\cdot}4H_2O$, was added while keeping the mixture at 57 °C. The evaporating process proceeded for 2 days until a viscous resin was formed. The resin was dried at 150 °C for 24 h and calcined in air at 700 °C. for 5 h.

2.2. Characterization

To assess the structural features of the perovskites, the solids were characterized as-synthesized, reduced and after catalytic tests by means of different techniques such as inductively coupled plasma emission spectroscopy (ICP), IR spectra, BET surface areas, X-ray diffraction experiments for crystalline phase detection and under temperature program reduction in H_2, temperature program reduction (TPR) and X-ray photoelectron spectroscopy (XPS) analyses. JCPDS-ICDD standard spectra software was used to determine the phases. The ruthenium crystallite size was calculated using Ru(1 0 1) reflection and the Scherrer equation [13,14]. The X-ray photoelectron spectroscopy (XPS) were performed with a VG ESCALAB 220 XL spectrometer. The monochromatic Al Kα (1486.6 eV) source was operated at 80 W. For the XPS analysis, the reduction treatments were conducted in situ using H_2 as reducing agent and left 9 h at 500 °C (heating rate 2 °C/min). Auto-coherent references were used: La $3d_{5/2}$ at 833.8 eV, Ru $3d_{5/2}$ at 280.2 eV and O 1s at 529.3 eV.

2.3. Activity test

Activity tests were performed using 200 mg of catalyst in a 20 mm i.d. quartz reactor at atmospheric pressure operated in a fixed-bed continuous flow system with $CH_4/CO_2 = 1$ for the dry reforming and $CH_4/CO_2/O_2 = 4/1/2$ for the combine reforming. Argon was used as diluent, 750–850 °C, and 24 L/(h g) hourly space velocities. Before the catalytic tests, the solids were reduced in H_2 flow (20 mL/min, T = 700 °C,

Table 1
BET surface area, IR bands, symmetry and cell prameters

Solids	SA (m^2/g)	IR bands		Sym	Cell parameter (Å)		
		ν_1	ν_2		*a*	*b*	*c*
$LaRuO_3$	2	612	414	O	5.58	7.67	5.54
$LaRu_{0.6}Ni_{0.4}O_3$	15	608	407	O	5.94	7.83	5.50
$LaRu_{0.4}Ni_{0.6}O_3$	17	626	400	O	5.54	7.88	5.94
$LaNiO_3$	14	595	420	T	10.42	10.43	6.92
$LaRu_{0.8}Ni_{0.2}O_3$	9	592	417	O	5.53	7.89	5.54
$La_{0.8}Ca_{0.2}Ru_{0.8}Ni_{0.2}O_3$	8	600	418	C	7.86	7.86	7.86
$La_{0.2}Ca_{0.8}Ru_{0.8}Ni_{0.2}O_3$	6	–	–	O	5.36	7.67	5.53
$CaRu_{0.8}Ni_{0.2}O_3$	3	–	–	O	5.36	7.66	5.53

Sym: symmetry; O: orthorombic; C: cubic; T: triclinic.

8 h). After reduction, the system was swept with Ar for 15 min and adjusted to reaction temperature. The water produced during reaction, was condensed before passing the reactants and products to the analyzing system, which consisted of an on-line gas chromatograph (Perkin Elmer Auto System XL) equipped with a TCD and provided with a Carbosieve SII 80/100 (12 in. × 1/8 in. o.d. SS). The conversions of CH_4 and CO_2 were defined as the converted CH_4 and CO_2 per total amount of CH_4 and CO_2 fed, respectively. The selectivity for product "i" was calculated based in carbon balance and defined as $S_i\,(\%) = (N_i/(NCH_4\ (c) + NCO_2\ (c))) \times 100$, where NCH_4 (c) and NCO_2 (c) are the amount of methane and carbon dioxide converted.

3. Results and discussion

3.1. Perovskites characterization: surface area, chemical analysis, IR and XRD

The chemical analysis of all synthesized perovskites showed a close similarity between analytical and nominal values, indicating the coincidence of real and nominal formula and the advantage of the sol–gel synthesis, as previously reported [1,2]. An oxygen deficiency was shown by most perovskites.

Table 1 lists the synthesized perovskites, their measured surface area, IR bands position, cell parameters and their corresponding symmetry. All synthesized solids showed two bands in the medium IR region at 600–500 and 400–450 cm^{-1} characteristics of the perovskite structure. Their positions are in good agreement with those reported in [1,5,15]. The position of the IR bands allows establishing the strength of B–O bond and its modification by substitution of the B cation. A compromise between the ease of reduction of the perovskite and its catalytic activity has been observed: catalytic activity being reverse to the ν_1 values.

BET specific surface areas measured after calcinations are in the order of 2–7 m^2/g, which are high compare to the usual values obtained for these solids [16].

The X-ray diffraction analysis of the as-synthesized solids at room temperature revealed that the perovskite structure was the main phase detected for all solids with high crystallinity and well-defined symmetry, in agreement with previously reported values [17,18]. Most perovskites could be indexed with an orthorhombic or cubic symmetry of the ABO_3 type (Table 1). TEM–EDX investigations performed on the fresh, reduced and used perovskite series revealed small and faceted metallic particles, given an average metallic dispersion for the series between 60% and 70%, except for the $LaRu_{0.4}Ni_{0.6}O_3$, where the dispersion was close to 9%.

In situ XRD and TPR analysis shown that as the temperature is raised, cations in B-site position are reduced to metals while those in A-site position are transformed to the respective oxides [1]. For all solids, the observed phases after reduction at 700 °C were: Ru metal (alone or allied with Ni), CaO and La_2O_3 depending on the composition of the starting solid. XRD analysis was also used to determine the metal particles size of the crystallites by means of the Scherrer equation [13,14]. Peaks correspond mainly to Ru (44.37°, 2θ) slightly shifted, due to the presence of Ni. For all structures, the calculated mean particle size values are between 10 and 15 nm (Table 2), indicating the existence of high dispersion and/or uniform distribution of Ru(Ni) in the CaO–La_2O_3 matrix. On the lanthanum containing perovskites, dioxomono carbonate, $La_2O_2CO_3$, was also observed. This layer is in fast equilibrium with the carbon dioxide in the gas phase during reaction, and has been claimed as responsible for inhibiting

Table 2
In situ XRD results: phases and average size of Ru(Ni) after reduction

Samples	2θ[a] (°)	*T* of degradation (°C)	Phases after reduction	Mean size (nm)
$LaRu_{0.8}Ni_{0.2}O_3$	32.100	400–500	Ru^0, Ni^0, La_2O_3	9.9
$La_{0.8}Ca_{0.2}Ru_{0.8}Ni_{0.2}O_3$	32.230	400–500	Ru^0, Ni^0, CaO, La_2O_3	10.3
$La_{0.2}Ca_{0.8}Ru_{0.8}Ni_{0.2}O_3$	32.486	300–500	Ru^0, Ni^0, CaO, La_2O_3	15.1
$CaRu_{0.8}Ni_{0.2}O_3$	32.912	300–400	Ru^0, Ni^0,CaO	14.9

[a] Evolution of the most intense peak at 29 °C.

Table 3
Ruthenium and oxygen XPS binding energy and composition

Perovskites	Ru		Oxygen	
	Fresh	Reduced	Fresh	Reduced
$LaRuO_3$	280.7 (weak)–282.35	280.4 (∼100%) + ε oxides	533.3 (11%)–532 (33%)–531 (33%)–529.5 (22.5%)	529.1 (25%)–531.1 (55%)–532.2 (20%)
$LaRu_{0.2}Ni_{0.8}O_3$	280.3 (∼33%)	282.5 (∼67%)	531.5 (44%)–529.4 (56%)	529.4 (62%)–531.5 (38%)
$LaRu_{0.4}Ni_{0.6}O_3$	282.4–283.6	280.3 (60%)–282.6 (40%)	531.8 (70%)–528.5 (13%)–529.4 (17%)	529.3 (56%)–531.4 (44%)
$LaRu_{0.6}Ni_{0.4}O_3$	282.9	280.4 (70%)–282.7 (30%)	532.9 (4%)–531.5 (63%)–528.5 (16%)–529.4 (16%)	529.3 (45%)–531.5 (55%)
$LaRu_{0.8}Ni_{0.2}O_3$	280.3 (∼33%)–282.5 (∼67%)	280.2 (70%)–281.7 (30%)	531.7 (80%)–529.5 (20%)	529.5 (22.5%)–530.9 (51.7%)–532.7 (5.8%)

formation of deactivating coke [19,20]. After 30 h of reaction, the TEM–EDX analysis showed that this layer remains in most of the solids [1,2]; however, was not detected after longer reaction periods, due essentially to carbon deposition.

3.2. X-ray photoelectron spectroscopy (XPS)

Table 3 lists the XPS composition for Ru and oxygen. Results showed that under the experimental conditions used only B-site cations (Ru and Ni) are reduced to the zero oxidation state, while those cations in A-site position do not show any reduction, as confirm by in situ XRD and TPR studies [1]. For the mixed $LaRu_{1-x}Ni_xO_3$ perovskite-type oxides, two well-defined peaks for Ru $3d_{5/2}$, one at ≈280 eV attributed to Ru^0 and a second one at ≈282.6 eV corresponding to unreduced Ru (Ru(III)) was observed. As the amount of Ni increases on the perovskites, the reducibility of Ru decreases. For the more active perovskite ($LaRu_{0.8}Ni_{0.2}O_3$), the signal attributed to Ru(III) appears at 281.7 eV indicating the existence of a different Ru species in this solid probably due to partially reduced Ru. Before reduction, Ru in $LaRuO_3$ and $LaRu_{0.8}Ni_{0.2}O_3$ appears mainly as oxide with a small amount of Ru metal. After reduction, the main phase is Ru metal with small amount of Ru oxide in different proportions, as seen in Table 3. The wider shape of the signal corroborated the presence of several Ru species in this solid.

Since activity of the perovskites is usually related to the mobility of oxygen on the solid, the chemical state of oxygen on the surface was also examined. Table 3 shows the oxygen XPS composition. Signals were assigned as: 529 eV to O^- of the perovskite lattice oxide; 531 eV to O^- bonded to La, Ru or Ni in an OH environment; ∼532 eV peroxides O_2^- or OH correspond to O less rich in electrons, weaker and more reactive [21].

Atomic ratios for $LaRu_xNi_{1-x}O_3$ series are shown in Table 4. As expected, some oxygen is lost after reduction. The Ru/La and Ni/La ratios are lower than the nominal value except for $LaRu_{0.6}Ni_{0.4}O_3$.

Table 5 shows the bulk and surface stoichiometry of the reduced $La_{1-x}Ca_xRu_{0.8}Ni_{0.2}O_3$ series perovskites. To evaluate the chemical state and evolution of the metals at the surface, a semi-quantitative analysis was performed. Only Ru/O and Ru/(A + A′) ratios are presented since attempts to extract reliable quantification of Ni was extremely difficult due to the severe covering of the Ni 2p signals by the complex La 3d region and the low nickel content on this series: $La_{1-x}Ca_xRu_{0.8}Ni_{0.2}O_3$ [1]. If it is assumed that for the Ca–La series Ru^0, CaO and La_2O_3 are the main phases present after reduction, as observed by XRD, the Ru/O ratio should be around three times smaller than that of Ru/La [22,23]. However, it is observed that the substitution of lanthanum by calcium lead to a Ru/O ratio approximately equal to that of Ru/La indicating a great deficiency in oxygen. These results are in good agreement with ICP and TPR observations, where the formation of an oxygen deficient perovskite of the type $La_{1-x}Ca_xRu_{0.8}Ni_{0.2}O_{3-\lambda}$ was invoked to compensate for the difference in charge produced when Ca^{2+} substitutes La^{3+}. In agreement with TPR and XRD results, the observed oxygen deficiency was lower for the most stable perovskite $LaRu_{0.8}Ni_{0.2}O_3$.

From the XPS results, the question of why $LaRu_{0.8}Ni_{0.2}O_3$ produces the most active catalyst is difficult to answer. However, there are some possibilities/causes to be considered:

Table 4
Atomic ratios

Solids	Ru/La		Ni/La		Ru + Ni/La	O/La	O/La	Ru/Ni
	Fresh	Red	Fresh	Red			Red	Red
$LaRuO_3$	0.3	0.28	–	–	0.3	3.1	1.74	∞
$LaRu_{0.8}Ni_{0.2}O_3$	0.10	0.15	0.07	0.08	0.23	3.1	1.34	2.29
$LaRu_{0.6}Ni_{0.4}O_3$	0.06	0.054	0.41	0.65	0.47	3.0	1.82	0.15
$LaRu_{0.4}Ni_{0.6}O_3$	0.06	0.054	0.25	0.29	0.31	2.84	1.5	0.2
$LaNiO_3$	–	–	0.5	0.55	0.5	3.68	1.9	0

Table 5
Bulk and surface stoichiometry of the reduced perovskites

Samples	La	Ca	Ru	Ni	O	Ru/O	Ru/(Ca + La)	(Ru/O)/(Ru/(Ca + La))
$LaRu_{0.8}Ni_{0.2}O_3$								
Surface	1.0	–	0.15	0.08	1.34	0.11	0.15	0.73
Bulk	1.0	–	0.80	0.20	3.00	0.27	0.80	0.34
$La_{0.8}Ca_{0.2}Ru_{0.8}Ni_{0.2}O_3$								
Surface	1.0	0.42	0.35	–	1.55	0.23	0.25	0.92
Bulk	0.8	0.270	0.80	0.20	3.00	0.27	0.80	0.34
$La_{0.2}Ca_{0.8}Ru_{0.8}Ni_{0.2}O_3$								
Surface	1.0	0.38	0.28	–	1.45	0.19	0.20	0.95
Bulk	0.2	0.80	0.80	0.20	3.00	0.27	0.80	0.34
$CaRu_{0.8}Ni_{0.2}O_3$								
Surface	0.0	1.00	0.22	0.17	0.94	0.23	0.22	0.96
Bulk	0.0	1.00	0.80	0.270	3.00	0.27	0.80	0.34

- The activity does not seem to be related to the amount of Ru at the surface since ($LaRuO_3$ has more Ru in the surface than $LaRu_{0.8}Ni_{0.2}O_3$).
- Since it is higher for $LaRu_{0.8}Ni_{0.2}O_3$, it could be related to Ru/Ni ratio.
- $LaRu_{0.8}Ni_{0.2}O_3$ is the only sample to show Ru $3d_{5/2}$ a 281.7 eV after reduction.
- Activity related to the quantity of Ru and/or Ni in the perovskite (oxide state)?
- The degree of reduction? Reduced $LaRu_{0.8}Ni_{0.2}O_3$ has the lower ratio O/La.
- Related to the presence of carbon or carbonate? $LaRu_{0.8}Ni_{0.2}O_3$ seems to have low carbon presence (C 1s ∼ 289–290 eV).
- Related to oxygen liability (O_2^- at 532.7 eV).

3.3. Catalytic studies

In previous work [1,2], the dry reforming of methane to syngas was carried out, optimizing reaction conditions to higher yields of syngas. It was found that the best Ru–Ni combination was obtained for $LaRu_{0.8}Ni_{0.2}O_3$ while on calcium containing perovskites $La_{0.8}Ca_{0.2}Ru_{0.8}Ni_{0.2}O_3$ produced higher ratio of H_2/CO. Calcium was used to increase the basicity of the catalysts in order to further inhibit coke formation. In the present work, the behavior of some of those precursor perovskites in the combine reforming of methane was studied.

Addition of oxygen to carbon dioxide reforming of methane can reduce the carbon deposition on the catalyst surface and increase methane conversion. This combine reaction emerges as an alternative of particular interest since it allows working at lower temperatures, due to the exothermic character of the partial oxidation reaction, which not only improves the H_2/CO ratio in the product, but traduces in lower energy consumption and a more economical way of methane conversion [7,24].

Table 6 compares the CH_4 and CO_2 conversions, CO selectivity, dispersion and carbon balance for La–Ru–Ni perovskite-type oxides. On these solids, steady state conditions for the perovskite oxide series were reached rapidly, remaining almost constant for up to 150 h, except for the $LaNiO_3$ solid which start loosing some activity after 100 h due essentially to carbon deposition on the Ni crystallites. With the exception of the $LaRuO_3$ solid, all perovskites showed a CH_4 conversion higher than that of CO_2 at all temperatures. This could imply that steam reforming of methane and/or methane cracking is taking place. When compared under isoconversion conditions, the $LaRu_{0.8}Ni_{0.2}O_3$ perovskite was the best precursor catalyst. The high activity shown by this solid is attributed to its higher metallic dispersion (89%) compare to $LaRu_{0.4}Ni_{0.6}O_3$ (9%), which showed the lower activity (see Table 6). The metal dispersion plays a fundamental role in these reactions as pointed out by Kim et al. for structure sensitive reactions [25].

For the Ca–La perovskites, under optimized experimental conditions, catalysts did not show significant coke deposition even after 120 h on stream (1.38% carbon/g of catalyst), maintaining their activity and selectivity to CO, which corroborate the low coke formed in these solids.

For the combine reaction, an important increase in CH_4 conversion at different temperatures was observed on $LaRu_{0.8}Ni_{0.2}O_3$, especially at lower temperatures (Fig. 1). Oxygen consumption was always 100%, in agreement with the results of Schmal and coworker on Pt supported catalysts [26]. Since the partial oxidation is an exothermic reaction, the energy liberated enhances the endothermic reaction favoring activity. However, the CO_2 conversion decreases for

Table 6
CH_4 and CO_2 conversions, CO selectivity, dispersion and carbon balance

Perovskite	C_{CH_4} (%)	C_{CO_2} (%)	S_{CO} (%)	Dispersion (%)	Carbon balance
$LaRuO_3$	57.8	67.5	86.2	68.2	98.1
$LaRu_{0.8}Ni_{0.2}O_3$	89.4	71.8	90.4	89.1	98.2
$LaRu_{0.6}Ni_{0.4}O_3$	64.9	60.4	82.3	56.3	94.7
$LaRu_{0.4}Ni_{0.6}O_3$	19.0	9.1	63.2	9.1	96.0
$LaNiO_3$	83.8	65.3	85.0	55.0	94.5

W = 200 mg, GHSV = 24 L/(h g), time on stream = 24 h, P = 1 atm, T = 923 K.

Table 7
CH_4 and CO_2 conversion, and H_2/CO ratio for dry and combine methane reforming

Solid	Dry reforming			Combine reforming		
	X (CH_4)	X (CO_2)	H_2/CO	X (CH_4)	X (CO_2)	H_2/CO
$LaRu_{0.8}Ni_{0.2}O_3$	79	81	0.94	87	51	1.18
$La_{0.8}Ca_{0.2}Ru_{0.8}Ni_{0.2}O_3$	68	62	0.86	83	50	1.18
$La_{0.2}Ca_{0.8}Ru_{0.8}Ni_{0.2}O_3$	46	50	0.87	88	47	0.86
$CaRu_{0.8}Ni_{0.2}O_3$	56	49	0.93	66	37	1.04

T_{reac} = 700 °C, WHSV = 24 L/(h g), CH_4/CO_2 = 1, CH_4/O_2 = 2, W = 200 mg, T_{red} = 700 °C/8 h, time on stream = 24 h.

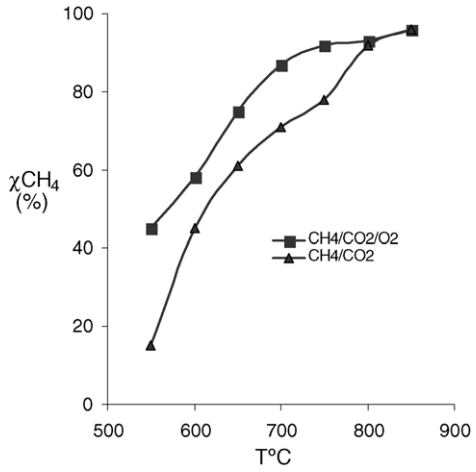

Fig. 1. CH_4 conversion vs. temperature on the dry and combine CH_4 reforming reaction on $LaRu_{0.8}Ni_{0.2}O_3$. tr = 24 h, WHSV = 24 L/(h g), CH_4/CO_2 = 1, CH_4/O_2 = 2, W = 200 mg, red = 700 °C/8 h.

all catalysts when O_2 is added to the system. This behavior could be explained by the fact that O_2 is a stronger oxidizing agent than CO_2 and its production is favored by reaction (7) where CO_2 is being generated as a product of the methane combustion in presence of O_2:

$$CH_4 + O_2 \leftrightarrow 2CO_2 + 2H_2 \quad (\Delta H_{298\,K} = -802\,kJ/mol) \quad (7)$$

When La is substituted by Ca, a decrease in both its activity and selectivity is observed, as shown in Table 7. This decrease is produced because the substitution of a cation of larger ionic radium by a smaller one induces changes in the perovskite needed for charge compensation as determined by ICP, TPR and XPS.

Oxygen addition to the $CH_4 + CO_2$ system, decreases the reaction temperature and the energy consumption, indicating that the partial oxidation (exothermic) reaction promotes the dry (endothermic) reaction, in accordance with observations of Tomishige et al. on Ni/Al_2O_3 and Pt/Al_2O_3 catalysts [8].

4. Conclusions

It was observed that preparation of the precursor perovskites by the sol–gel method produces solids with high homogeneity and crystallinity which showed a well-defined perovskite structure as confirmed by the different characterization techniques. TEM–EDX analysis and XRD studies performed on the $LaRu_{1-x}Ni_xO_3$ series revealed the complete destruction of the perovskite with reduction of Ru and/or Ni. During reaction, formation of small and faceted metallic particles with dispersions between 60% and 70% was observed, together with the existence of a significant amount of a $La_2O_2CO_3$ phase, especially on the $LaRu_{0.8}Ni_{0.2}O_3$. Reduction before reaction of the precursor perovskites produced small metallic particles that avoid coke formation and give rise to active and stable catalysts. Due to the stability shown by these solids, it is believed that this phase highly contributed to the resistance to deactivation.

All perovskites oxides, except $LaRu_{0.4}Ni_{0.6}O_3$ were found to be highly active toward the syngas production during the CO_2 reforming of methane. Among the solids tested, the $LaRu_{0.8}Ni_{0.2}O_3$ showed a high potential as a catalyst for this reaction, reaching conversions of 89% and 72% in CH_4 and CO_2, respectively, with CO selectivity close to 90% even after 150 h on stream.

The simultaneous oxidative and CO_2 reforming reaction of methane notably diminish coke formation, increasing activity and syngas production at lower temperature.

Acknowledgements

The authors are grateful to FONACIT for financial support through Agenda Petroleum Project Nos. 97-003739 and PICS PI 2003000024.

References

[1] M.R. Goldwasser, M.E. Rivas, E. Pietri, M.J. Pérez-Zurita, M.L. Cubeiro, L. Gingembre, L. Leclercq, G. Leclercq, Appl. Catal. A: Gen. 255 (2003) 45.
[2] E. Pietri, A. Barrios, O. Gonzalez, M.R. Goldwasser, M.J. Pérez-Zurita, M.L. Cubeiro, J. Goldwasser, L. Leclercq, G. Leclercq, Stud. Surf. Sci. Catal. 136 (2001) 381.
[3] J.B. Wang, S.-Z. Hsiao, T.-J. Huang, Appl. Catal. A: Gen. 246 (2003) 197.
[4] T. Hayakawa, S. Suzuki, J. Nakamura, T. Uchijima, S. Hamakawa, K. Suzuki, T. Shihido, K. Takehira, Appl. Catal. A: Gen. 183 (1999) 273.
[5] E. Pietri, A. Barrios, M.R. Goldwasser, M.J. Pérez-Zurita, M.L. Cubeiro, J. Goldwasser, L. Leclercq, G. Leclercq, L. Gingembre, Stud. Surf. Sci. Catal. 30 (2000) 3657.
[6] M.A. Peña, J.L.G. Fierro, Chem. Rev. 101 (2001) 1981.

[7] V. Szabo, M. Bassir, A. Van Neste, C. Kaliaguini, Appl. Catal. B: Environ. 43 (2003) 29.
[8] K. Tomishige, S. Kanazawa, K. Suzuki, M. Asadullah, M. Sato, K. Ikushima, K. Kunimori, Appl. Catal. A: Gen. 233 (2002) 35.
[9] M.R. Goldwasser, V.E. Dorantes, M.J. Pérez-Zurita, P.R. Sojo, M.L. Cubeiro, E. Pietri, F. González-Jiménez, Y. Ng Lee, D. Moronta, J. Mol. Catal. A: Gen. 3790 (2002) 1.
[10] D.L. Trimm, Catal. Today 49 (1999) 3.
[11] O.V. Krylov, A.Kb. Mamedov, S.R. Mirzabekova, Catal. Today 42 (1998) 211.
[12] K. Tomishige, O. Yamazaki, Y. Chen, K. Vokoyama, X. Li, K. Fujimoto, Catal. Today 45 (1998) 35.
[13] M.C.J. Bradford, M.A. Vannice, Appl. Catal. A: Gen. 142 (1996) 73.
[14] H.P. Klug, L.E. Alexander, X-ray Diffraction Procedures for Polycrystalline and Amorphous Materials, Wiley, London, 1962.
[15] C.P. Khattak, D.E. Cox, Mater. Res. Bull. 12 (1977) 463.
[16] J.M.D. Tascón, S. Mendioróz, L. González Tejuca, Z. Phys. Chem. 124 (1981) 109.
[17] J.B.A. Elermans, B. VanLaar, K.R. Vander Veen, B.O. Loopstra, J. Solid State Chem. 3 (1971) 238.
[18] A. Slagtern, Y. Schuurman, C. Leclercq, X. Verykios, C. Mirodatos, J. Catal. 172 (1997) 118.
[19] N. Matsui, K. Anzai, N. Akamatsu, K. Nakagawa, N. Okikenaga, T. Suzuki, Appl. Catal. A: Gen. 179 (1999) 247.
[20] V.A. Tsipouriari, X.E. Verykios, Catal. Today 64 (2001) 83.
[21] Q. Xu, D.-P. Huang, W. Chen, H. Wang, B.-T. Wang, R.Z. Yuan, Appl. Surf. Sci. 228 (1–4) (2004) 110.
[22] J.A. Marcos, R.H. Buitriago, E.A. Lombardo, J. Catal. 105 (1987) 95.
[23] H. Falcón, M.J. Martinez-Lope, J.A. Alonso, J.L.G. Fierro, Appl. Catal. B: Environ. 26 (2000) 131.
[24] Z. Zhong, K. Chen, Y. Ji, Q. Yan, Appl. Catal. A: Gen. 156 (1997) 29.
[25] G.J. Kim, D. Cho, K. Kim, J. Kim, Catal. Lett. 28 (1994) 41.
[26] M.M.V.M. Souza, M. Schmal, Catal. Lett. 91 (2003) 11.